Liquid Crystals
Publication details, including instructions for authors and subscription information:
http://www.informaworld.com/smpp/title~content=t713926090

Synthesis of macrocyclised dimetric compounds and their liquid crystal transition behaviours

Manabu Itoh[a]; Masatoshi Tokita[a]; Kaoru Adachi[a]; Teruaki Hayakawa[a]; Sungmin Kang[a]; Yasuyuki Tezuka[a]; Junji Watanabe[a]
[a] Department of Organic and Polymeric Materials, Tokyo Institute of Technology, Ookayama, Meguro-ku, Tokyo, Japan

Online publication date: 14 December 2009

To cite this Article Itoh, Manabu , Tokita, Masatoshi , Adachi, Kaoru , Hayakawa, Teruaki , Kang, Sungmin , Tezuka, Yasuyuki and Watanabe, Junji(2009) 'Synthesis of macrocyclised dimetric compounds and their liquid crystal transition behaviours', Liquid Crystals, 36: 12, 1443 — 1450
To link to this Article: DOI: 10.1080/02678290903288011
URL: http://dx.doi.org/10.1080/02678290903288011

Liquid Crystals,
Vol. 36, No. 12, December 2009, 1443–1450

Taylor & Francis
Taylor & Francis Group

Synthesis of macrocyclised dimetric compounds and their liquid crystal transition behaviours

Manabu Itoh, Masatoshi Tokita*, Kaoru Adachi†, Teruaki Hayakawa, Sungmin Kang, Yasuyuki Tezuka and Junji Watanabe

Department of Organic and Polymeric Materials, Tokyo Institute of Technology, Ookayama, Meguro-ku, Tokyo 152-8552, Japan

(Received 17 June 2009; final version received 25 August 2009)

Cyclic C-*n* dimers were synthesised by the ring-closing metathesis of linear L-*n* dimers with allyl tails under high dilution in the presence of the first Grubbs catalyst. The C-*n* dimers form a smectic phase similarly to the precursor L-*n* dimers, but the smectic structure and phase transition behaviour are remarkably different from those in L-*n* in the following respects. First, the C-*n* dimers invariably form a smectic A phase, although the L-*n* dimers as well as the conventional dimers form smectic A and smectic CA phases depending on whether the number of carbons on the spacer is even or odd. Second, the isotropisation temperature of the C-*n* dimer is significantly higher than that of the L-*n* dimer so that the smectic temperature span is expanded to 100°C from around 30°C for L-*n*. Third, the layer order in the smectic phase of the C-*n* dimer is remarkably higher than that of the L-*n* dimer, especially when *n* is small. These differences are explained as an effect of macrocyclisation, which forces the spacer to fold and thereby causes the two mesogens within a molecule to face each other closely.

Keywords: liquid crystalline dimer; macrocyclisation; ring-closing metathesis; cyclic dimer; smectic phase

1. Introduction

Twin dimers forming liquid crystals (LCs) are composed of two mesogenic units linked by a flexible methylene spacer. The dimers exhibit characteristic oscillations in the temperature and entropy of the LC-isotropic transition depending on the parity of the number of methylene units in the spacer, *n*: those of the dimer with even *n* are higher than the homologues with odd *n* (*1–3*). If the dimer forms a smectic mesophase, odd–even oscillation also appears in the type of smectic phase: while the homologues with even *n* form a smectic A (SmA) phase, the homologues with odd *n* form a smectic CA (SmCA) phase (*2*, *3*).

In the smectic phases, the LC dimers confront another intrinsic problem in terms of the accommodation of the two kinds of aliphatic parts, that is, the spacer and an alkyl tail attached to the mesogen, between the aromatic layers. Two types of accommodation of the aliphatic parts have been confirmed. One is the single-layer smectic (Sm^s) phase constructed by random mixing of the two aliphatic parts, and the other is the bilayer smectic (Sm^b) phase in which the two groups are segregated (*4*). While the Sm^s phase tends to be formed by dimers having a spacer with a length comparable to twice the length of the tail, the Sm^b phase has been observed for dimers having a tail much longer than the spacer. Recently, another way to accommodate the longer tail has been found for homologous LC dimers having a 3-methylpentane spacer and an alkyl tail with a carbon number larger than 12 (*5*). Such dimers form a SmA phase in contrast to dimers with pentane spacers, which assume an extended conformation and form a bilayer SmCA ($SmCA^b$) phase (*4*). The SmA phase has been presumed to be composed of dimers with the spacer folded to arrange the two mesogens parallel to each other.

In this work, we prepared cyclic dimers in which the spacers are folded between the mesogens to form an LC, and examined their characteristic LC properties. First, dimers (L-*n*) having two allyl tails with -CH=CH_2 groups at the ends were synthesised and then their tails were connected by ring-closing metathesis under high dilution in the presence of the first Grubbs catalyst to obtain macrocyclised dimers (C-*n*). C-*n* as well as the precursor linear dimers (L-*n*) form isotropic, smectic and crystalline phases in order of decreasing temperature. The thermotropic phase behaviour and the mesophase structure characteristic of the C-*n* dimers are presented in comparison with those of the L-*n* dimers.

2. Experimental procedure

2.1 Synthesis of materials

Figure 1 outlines a typical synthetic route leading to cyclic dimeric LCs. The synthetic route to the target compounds is as follows. 4′-(4-Penten-1-yloxy) biphenyl-4-carboxylic acid (**2**) was prepared by the etherification of 4′-hydroxy-4-biphenylcarboxylic acid (**1**). L-*n* (**3**) was obtained by the esterification of **2** with the corresponding α, ω-dihydroxyalkane. Macrocyclic

*Corresponding author. Email: mtokita@polymer.titech.ac.jp

†Present address: Department of Chemistry and Materials Technology, Kyoto Institute of Technology, Kyoto, Japan.

ISSN 0267-8292 print/ISSN 1366-5855 online

DOI: 10.1080/02678290903288011
http://www.informaworld.com

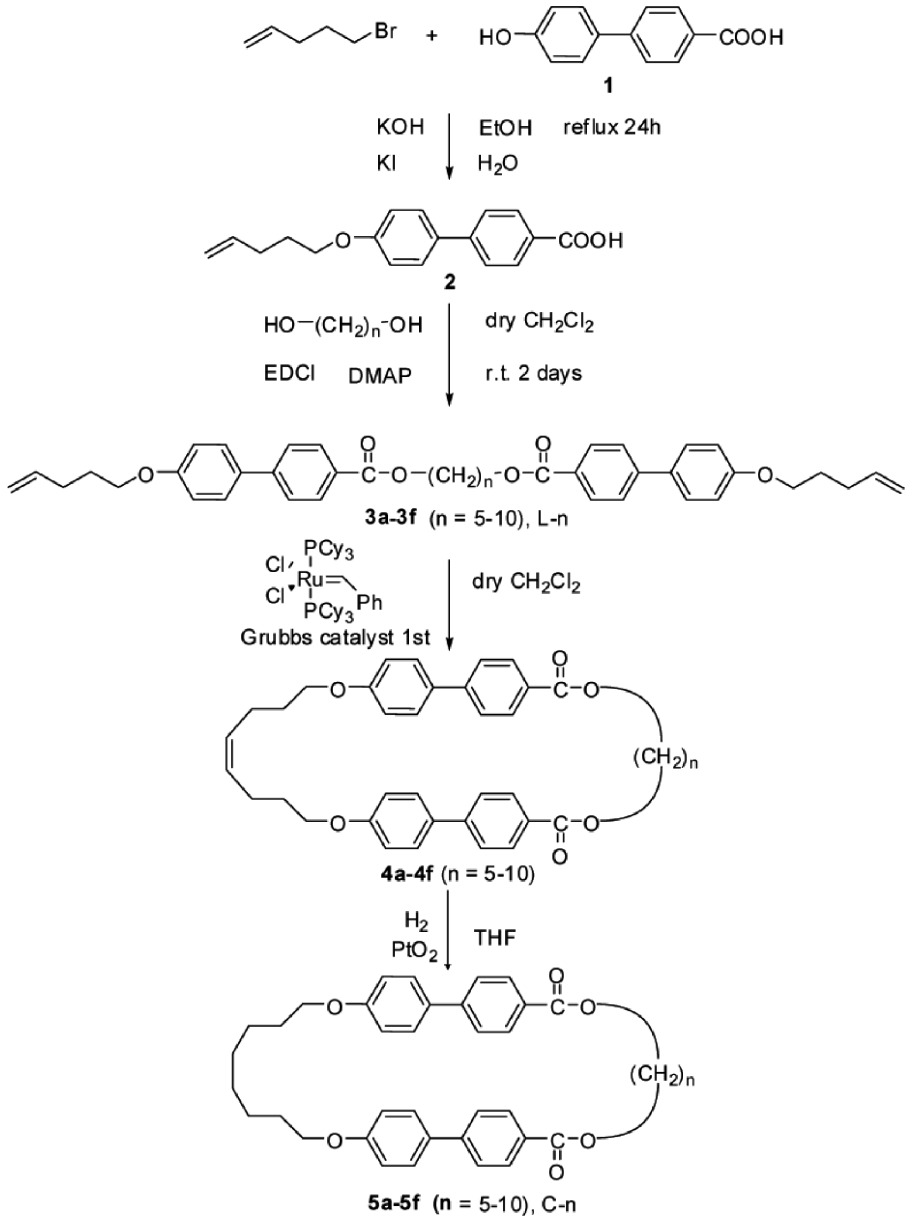

Figure 1. Synthetic route leading to linear (L-*n*) and macrocyclic (C-*n*) liquid crystalline dimers.

C-*n* dimers (**5**) were synthesised by ring-closing metathesis of the L-*n* dimers under high dilution (*6–8*). All reagents were purchased from TCI (Tokyo Kasei Kogyo Co., Ltd.), Aldrich and Wako and were used without further purification. Solvents were purified by normal procedures and handled under a moisture-free atmosphere. ^{1}H-nuclear magnetic resonance (NMR) spectra were recorded on a JEOL FT-NMR AL400 (400 MHz) spectrometer using tetramethylsilane as an internal standard. Matrix-assisted laser desorption/ionisation (MALDI)/time-of-flight (TOF)/mass spectrometry (MS) spectra were taken on an AXIMA-CFR mass spectrometer (Shimazu).

2.1.1 Synthesis of 4′-(4-Penten-1-yloxy) biphenyl-4-carboxylic acid, ***2***

4′-Hydroxy-4-biphenylcarboxylic acid (**1**) (3.0 g, 14.0 mmol) was dissolved with potassium hydroxide (1.77 g, 31.5 mmol) and potassium iodide (0.1 g) in a mixture of ethanol (60 ml) and water (20 ml). 5-Bromo-1-pentene (2.23 g, 15.0 mmol) was dropped into the solution and the mixture was refluxed for 24 h. The solution was cooled, poured into 200 ml of water, and acidified with concentrated hydrochloric acid. The solid carboxylic acid was removed by filtration and washed with water. The crude product was recrystallised from acetic acid to give **2** (2.93 g,

73.5%) as white plates. ^{1}H-NMR (DMSO-d_6): δ7.98 (2H, m, H3, H5-biphenyl), 7.74 (2H, m, H2, H6-biphenyl), 7.67 (2H, m, H2′, H6′-biphenyl), 7.04 (2H, m, H3′, H5′-biphenyl), 5.93–5.83 (1H, m, vinyl H), 5.04 (1H, m, vinyl H), 4.04 (2H, t, J = 6.5 Hz, CH_2O), 2.23–2.17 (2H, m, CH_2=CHC$\underline{H}_2$), 1.87–1.80 (2H, m, $OCH_2C\underline{H}_2$).

2.1.2 *Synthesis of L-n dimer, 3*

Here the synthesis route for the L-6 dimer (**3b**) is described. To a solution of 1,6-hexanediol (0.123 g, 1.04 mmol) in CH_2Cl_2 (50 ml) we added 1-ethyl-3-(3-dimethylaminopropyl) carbodiimide hydrochloride (0.659 g, 3.44 mmol), 4-dimethylaminopyridine (0.280 g, 2.29mmol), and 4′-(4-penten-1-yloxy)biphenyl-4-carboxylic acid, **2** (0.646 g, 2.29 mmol). The mixture was stirred at room temperature for 2 days. The reaction mixture was evaporated under reduced pressure and poured into methanol. The precipitate was filtered and recrystallised from chloroform/ethanol to give L-6 dimer **3b** (0.56 g, 83.8%) in the form of white crystals. L-5 (**3a**), L-7 (**3c**), L-8 (**3d**), L-9 (**3e**) and L-10 (**3f**) dimers were similarly prepared with 61.9%, 84.7%, 84.4%, 66.9% and 59.1% yields, respectively. For **3b**, ^{1}H-NMR ($CDCl_3$): δ8.06 (4H, d, J = 8.3 Hz, H3, H5-biphenyl), 7.59 (4H, d, J = 8.3 Hz, H2, H6-biphenyl), 7.53 (4H, d, J = 9.4 Hz, H2', H6'-biphenyl), 6.97–6.94 (4H, m, H3′, H5′-biphenyl), 5.92–5.82 (2H, m, vinyl H), 5.11–5.01 (4H, m, vinyl H), 4.38 (4H, t, J = 6.3 Hz, $COOCH_2$), 4.02 (4H, t, J = 6.5 Hz, OCH_2), 2.27 (4H, q, J = 7.2 Hz, CH_2=CHC$\underline{H}_2$), 1.95–1.85 (8H, m, $OCH_2C\underline{H}_2$, $COOCH_2C\underline{H}_2$), 1.70–1.65 (4H, m, $COOCH_2CH_2C\underline{H}_2$). The spectrum is shown later in Figure 9(a).

2.1.3 *Synthesis of C-n dimer,* ***5***

The cyclisation of L-*n* (**3**) was performed under reflex in dry CH_2Cl_2 at a concentration of 0.2 g L^{-1} in the presence of the first Grubbs catalyst. The catalyst was charged in a double molar quantity to allyl groups at the linear dimer tail. After evaporation of the solvent under reduced pressure, the concentrated solution was recovered by alumina flash chromatography to remove the catalyst residues. The product was purified by separation gel permeation chromatography and recrystallised from chloroform and ethanol. The cyclic structure of **4** was confirmed by MALDI/TOF/MS with the corresponding peak. As seen in Figure 2, the MS measured for 4b includes the corresponding peak at m/z = 642.0 $[M+Na]^+$ and the peak attributed to the cyclic tetramer is not found in the scanning range up to m/z = 2000. **4** was hydrogenated in tetrahydrofuran under H_2 atmosphere in the presence of Adams' catalyst (PtO_2). The reaction solution was

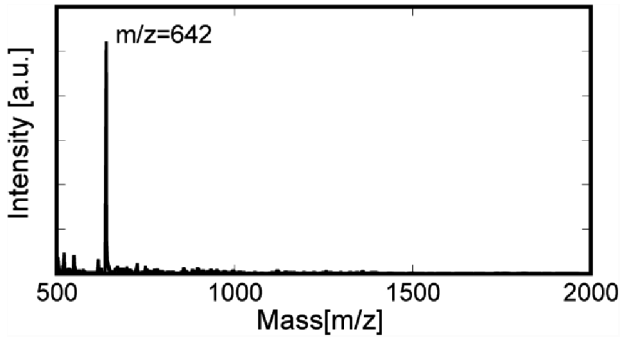

Figure 2. Matrix-assisted laser desorption/ionisation/time-of-flight/mass spectrometry spectra of **4b** (linear mode, matrix: dithranol with sodium trifluoroacetate).

filtered by celite545 to remove the catalyst residues and then evaporated. The residue was recrystallised from toluene and hexane to give C-6 dimer **5b** (15.4 mg, 52.8%) as white needles. The absence of the resonances of molecular ends of -CH=CH_2 in ^{1}H-NMR spectra establishes the cyclic structure of C-*n*. For C-6 (**5b**), ^{1}H-NMR ($CDCl_3$): δ8.00–7.98 (4H, m, H3, H5-biphenyl), 7.45–7.40 (4H, m, H2, H6-biphenyl), 7.33–7.30 (4H, m, H2′, H6′-biphenyl), 6.82–6.79 (4H, m, H3′, H5′-biphenyl), 4.40 (4H, t, J = 5.5 Hz, $COOCH_2$), 4.01 (4H, t, J = 6.1 Hz, OCH_2), 1.87–1.86 (2H, m, CH_2), 1.83–1.76 (2H, m, CH_2), 1.70–1.67 (2H, m, CH_2), 1.52–1.51 (2H, m, CH_2), 1.44–1.42 (2H, m, CH_2). The spectrum is shown in Figure 9(b).

2.2 *Methods*

The optical textures of mesophases were observed using an Olympus BX-51 polarised optical microscope equipped with a Mettler FP-82 hot stage. Differential scanning calorimetry (DSC) measurements were carried out with a Perkin-Elmer DSC-7 at a scanning rate of 10°C min^{-1}. Wide-angle X-ray diffraction measurements were conducted with a Laue camera using graphite monochromated Cu Kα radiation generated by a Rigaku UltraX18 generator. The diffraction pattern was recorded on a flat imaging plate. The temperature of the sample was regulated within 0.1°C by a Mettler FP-82 hot stage.

3. Results and discussion

L-*n* and C-*n* dimers with n = 5–10 undergo the well-defined thermotropic LC transitions. The transition temperatures and their related thermodynamic parameters are listed in Table 1.

Figure 3(a) shows the variation of the transition temperature with *n* observed in L-*n* dimers. All dimers commonly form a smectic phase, but the smectic structure depends on the odd–even parity of *n*. The formation of different smectic phases can be easily detected

Table 1. Thermodynamic data for L-*n* and C-*n* dimers.

	Phase sequence and transition temperatures (°C)							ΔH_i (kJ mol^{-1})	ΔS_i (J mol^{-1} K^{-1})
L-5	Cr			131.6	SmCA	141.0	Iso	15.6	37.6
L-6	Cr			136.6	SmA	167.7	Iso	23.1	52.4
L-7	Cr	95.4	SmX	99.6	SmCA	130.5	Iso	17.0	42.1
L-8	Cr	123.5	SmX	126.4	SmA	154.6	Iso	22.0	51.4
L-9	Cr	90.6	SmX	93.6	SmCA	123.0	Iso	15.9	40.0
L-10	Cr	108.6	SmB	113.8	SmA	142.6	Iso	24.5	58.9
C-5	Cr			183.4	SmA	277.8	Iso	15.9	28.8
C-6	Cr			169.2	SmA	228.9	Iso	10.9	21.7
C-7	Cr	120.2	SmX	130.4	SmA	231.2	Iso	11.7	23.2
C-8	Cr			94.0	SmA	184.1	Iso	8.3	18.2
C-9	Cr	92.2	SmX	95.8	SmA	193.5	Iso	10.0	21.3
C-10	Cr			79.3	SmA	152.6	Iso	6.4	15.0

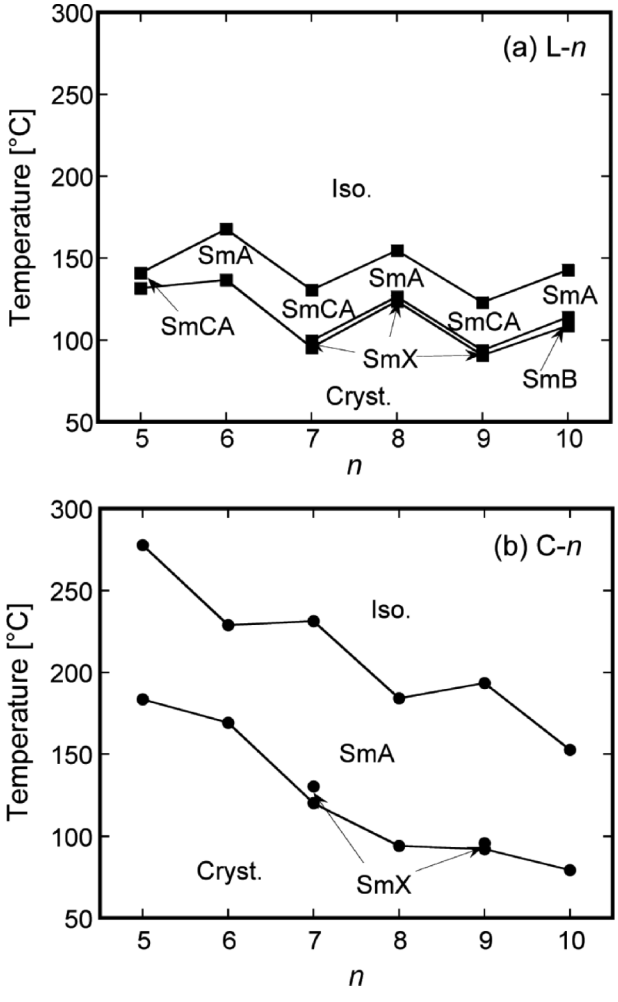

Figure 3. Dependence of transition temperatures for (a) L-*n* dimers and (b) C-*n* dimers on the number of methylene units in the spacer moiety (*n*). The transition temperatures were determined by differential scanning calorimetry thermograms at a cooling rate of 10°C min^{-1}.

by polarised optical microscopy (POM). L-*n* dimers with even *n* exhibit typical batonnets at the isotropic-LC transition, which coalesce to form a fan-shaped texture. By sliding the cover glass after the completion of LC formation, the fan-shaped texture is altered to a homeotropic dark texture. These characteristic textures are produced by the SmA structure. Under the same conditions, L-*n* dimers with odd *n* exhibit spherulite and Schlieren textures, which are characteristic of the SmCA phase. Thus, L-*n* with even *n* form the SmA phase while L-*n* with odd *n* form the SmCA phase, as has been commonly observed in smectic LC dimer systems. In line with the odd–even alternation of the type of smectic phase, the smectic layer spacing of L-*n* oscillates depending on the parity of *n*; the smectic layer spacing of L-*n* with even *n* is longer than that of L-*n* with odd *n* although both increase with *n* (see Figure 4). The layer spacing is comparable to half the molecular length calculated in an extended conformation, indicating that the smectic layer is formed by random mixing of the tail and spacer moieties. The smectic phases are thus assigned to Sm^s phases; namely, SmA^s for even L-*n* and SmCA^s for odd L-*n* (see Figures 5(a) and (b)). Whilst the smectic phases of L-*n* with $n = 5$ and 6 crystallised on cooling, L-*n* with $n = 7$–10 formed another mesophase over a narrow temperature range without showing a significant change in optical texture according to POM observation. The type of mesophase is smectic B for L-10 but it remains unclear for other dimers.

In contrast to L-*n* dimers, C-*n* dimers invariably form the SmA phase, which is also identified using the POM. Decisive evidence for the formation of the SmA phase is given by the X-ray diffraction pattern in Figure 6, which includes inner smectic layer reflections on the meridian line and outer diffuse halos on the equatorial line. In Figure 4, the layer spacing of the SmA phase is plotted as closed circles against *n*. It increases monotonically with *n* without oscillation,

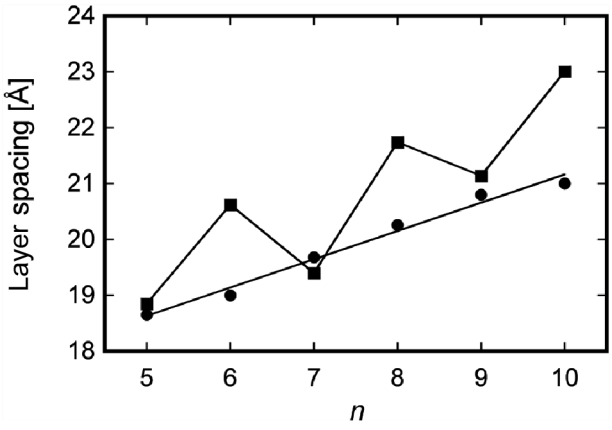

Figure 4. Variation of smectic layer spacing with n for L-n (square) and C-n (circle) dimers.

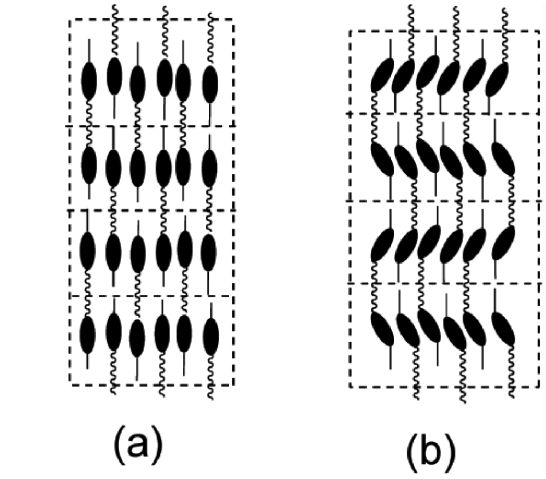

Figure 5. Schematic representation of smectic structures formed by L-n and C-n dimers: (a) SmA^s structure formed by L-n dimers with even n; (b) $SmCA^s$ structure formed by L-n dimers with odd n.

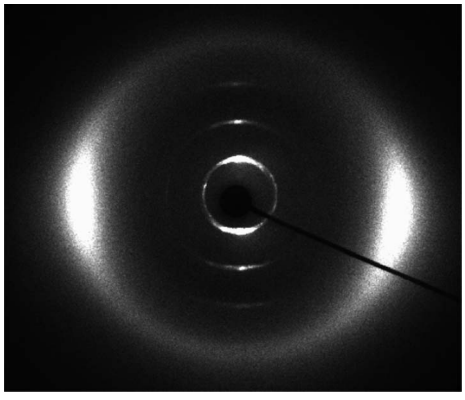

Figure 6. Two-dimensional X-ray diffraction patterns measured for the SmA phase of the C-7 dimer.

showing the maintenance of the SmA structure with the variation of n. The change in the layer spacing from 18.5 to 21.0 Å with increasing n from 5 to 10 is comparable to that observed in L-n dimers. The slope of the line indicates that the spacing increases by 0.5 Å with increments of n, which is also comparable to that in L-n dimers. Extrapolation of n to zero gives a value of 16 Å. All these values are reasonable when the cyclic molecules are assumed to have a hairpin folding structure, where the two alkyl spacers take a hairpin folding conformation and the two mesogens linked by these spacers face each other at a short distance and arrange their long axis in one direction. A typical example of a folding chain is given in Figure 7(a), and the resulting SmA structure is illustrated in Figure 7(b).

In addition to the absence of the odd–even effect on the smectic structure, the C-n dimers exhibit distinct thermodynamic parameters associated with the isotropisation of the SmA phase. First, the isotropisation temperature T_i for C-n is distinctly higher than that for L-n and decreases with increasing n to asymptotically approach T_i for L-n. As a result of the elevation of T_i, the smectic temperature zone for C-n becomes wider than that for L-n; the temperature span for C-n is approximately 100°C, while it is about 30°C for L-n (compare Figures 3(a) and (b)). Furthermore, T_i for C-n with odd n is higher than that for C-n with even n; this oscillation is opposite to that observed for L-n. Second, the isotropisation enthalpies (ΔH_i) and entropies (ΔS_i) are markedly smaller than those for L-n; for example, ΔS_i for C-10 is approximately one-quarter of that for L-10. Note here that the dependence of these parameters on n also shows a distinct trend from that observed for L-n (see Table 1 and Figure 8). ΔH_i and ΔS_i for L-n with

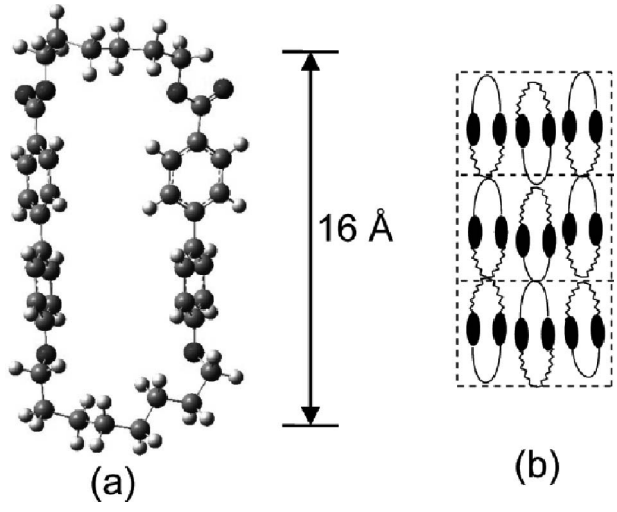

Figure 7. (a) Possible conformation of the C-6 dimer ; (b) schematic illustration of the SmA structure formed by C-n dimers.

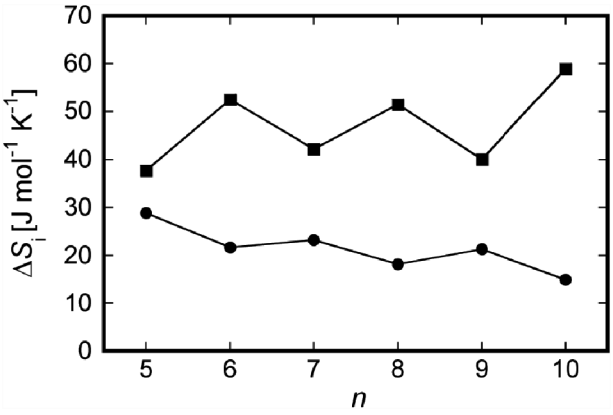

Figure 8. Dependence of isotropisation entropy ΔS_i on n for L-n (squares) and C-n (circles) dimers.

even n are larger than those for L-n with odd n; both values increase slightly with n. In contrast, ΔH_i and ΔS_i for C-n decrease with n and exhibit a weak odd–even oscillation, which is the opposite of that observed for the L-n dimers. We cannot find any reason why macrocyclisation induces the inversion of the odd–even oscillations in these thermodynamic parameters. Such an enlargement of LC temperature zone has been observed for macrocycles combining two biphenyl units (*9–11*). The increase in T_i and the decrease in ΔS_i by cyclisation have also been reported for macrocyclic main-chain LC polymers (*12*).

Assuming that the molecular conformation in the isotropic melt may be diverse to a similar extent to that in the solution, the conformation was examined using ^{1}H NMR spectra of the solution. Figures 9(a) and (b) show the ^{1}H-NMR spectra of the L-6 and C-6 dimers, respectively. The most significant difference between L-6 and C-6 is observed in the chemical shifts of the aromatic protons. In Figure 10, the chemical shifts of the aromatic protons are plotted as a function of n for both C-n and L-n. It can be clearly seen that the chemical shifts are independent of n for L-n dimers, while those for C-n dimers shift upfield by 0.1–0.2 ppm from those for L-n dimers. Such upfield shifts for C-n have been explained as being caused by the aromatic ring current, showing that the two aromatic rings of the macrocyclic dimer face each other at a short distance in solution (*12*, *13*). Therefore, even in the isotropic solution (or liquid), the cyclic dimers assume confined conformations, which have a side-by-side arrangement of the two aromatic groups. This conclusion is reliable since the limited length of the spacer linking the two mesogens significantly confines the angular distribution of the two mesogens as well as the distance between the two mesogens. In fact, conformational analysis by quantum chemistry calculations shows that the two aromatic mesogens in the possible conformations face each other at a short distance with a wide axial correlation. These arrangements are schematically illustrated in Figure 11(a). Thus, the isotropic to smectic transition is followed by the selection of conformers in which the mesogens are uniaxially aligned from the limited number of conformers (see Figure 11(b)). This is the reason why ΔS_i for C-n is smaller than that for L-n. From Figure 10, it is also found that the upfield shifts of the aromatic protons in C-n exhibit an odd–even oscillation that decreases with n. The higher the shifts in even C-n, the more close-facing the aromatic rings, or the more limited the conformers in the isotropic solution. This result may be related to the odd–even oscillation of ΔS_i.

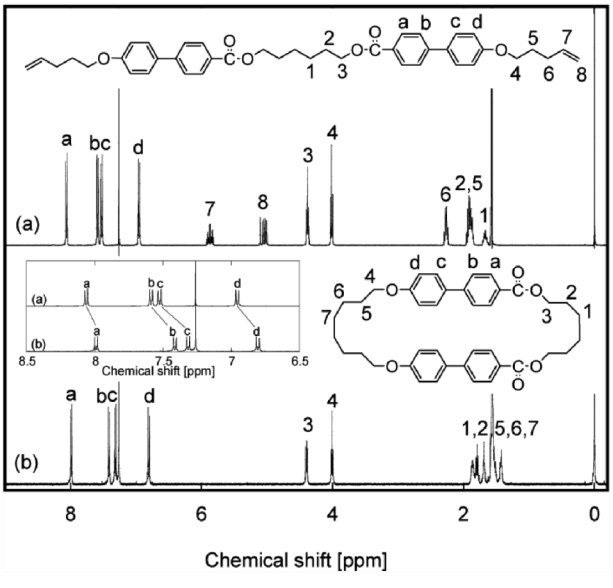

Figure 9. ^{1}H-nuclear magnetic resonance spectra of (a) L-6 and (b) C-6 dimers.

Finally, we note that the entropy change in C-n definitely decreases with increasing n, although the decrease is relatively small. This dependence, opposite to that conventionally observed, is unusual, since the increase in the flexible chain length generally increases the number of conformations in the isotropic state, which increases the entropy change upon the isotropisation of the LC. This unusual trend in the C-n dimers may be associated with the layer order of the smectic structure, which is related to the ratios among the integrated intensities of the lth-order layer reflections $I(00l)$ in the X-ray diffraction pattern (*14*). Figure 12 shows the n dependence of the intensity ratios of $I(002)/I(001)$ for both C-n and L-n dimers. For C-n dimers, $I(003)/I(001)$ ratios are also presented since the (003) reflection has a relatively strong intensity. From this figure, we found that $I(002)/I(001)$ for L-n is relatively small and its dependence on n is negligibly weak.

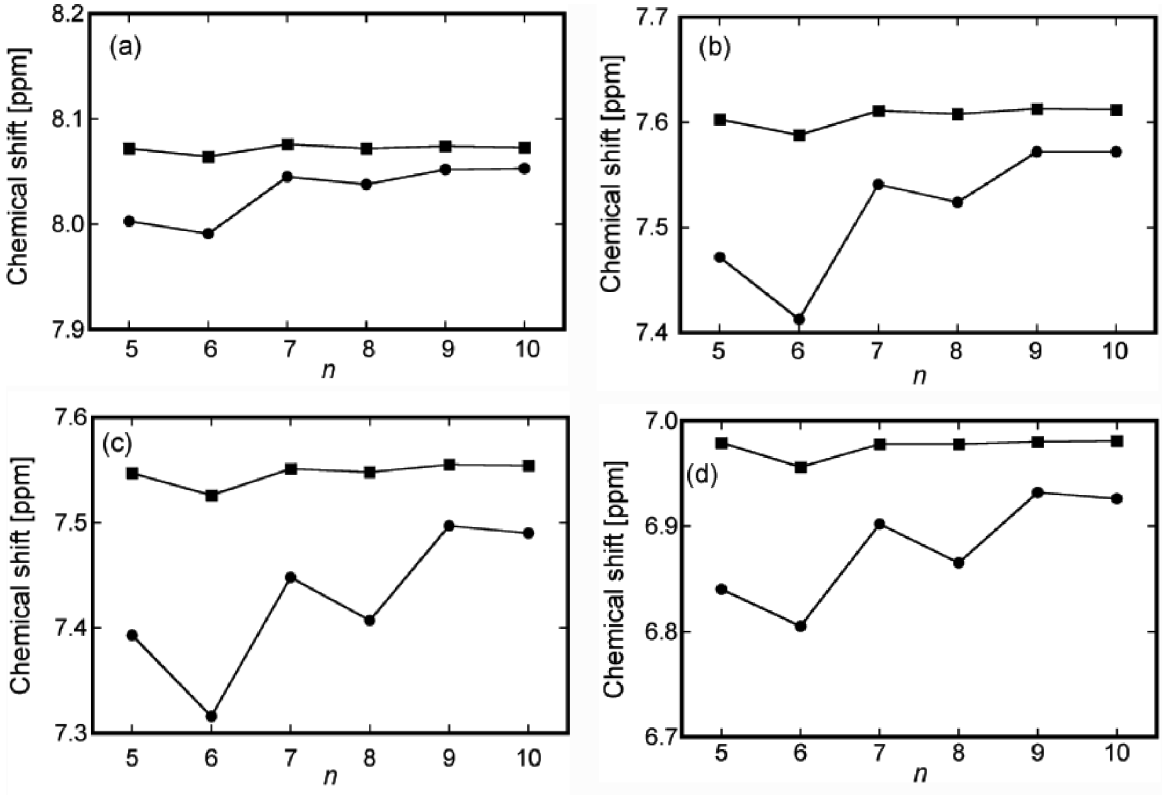

Figure 10. Variations of the chemical shifts of aromatic protons of L-*n* (squares) and C-*n* (circles) dimers with *n*. The assignments of the protons are shown in Figure 9.

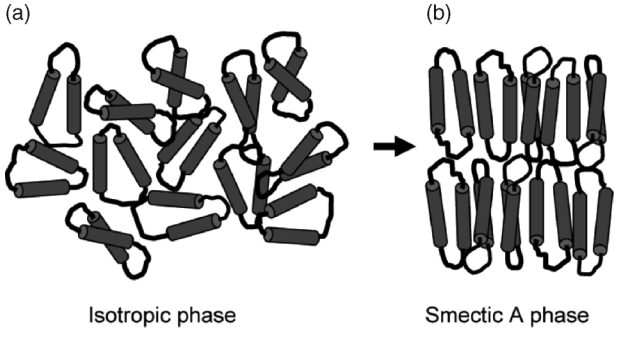

Figure 11. Schematic illustration of C-*n* molecules in (a) the isotropic phase and (b) the smectic phase.

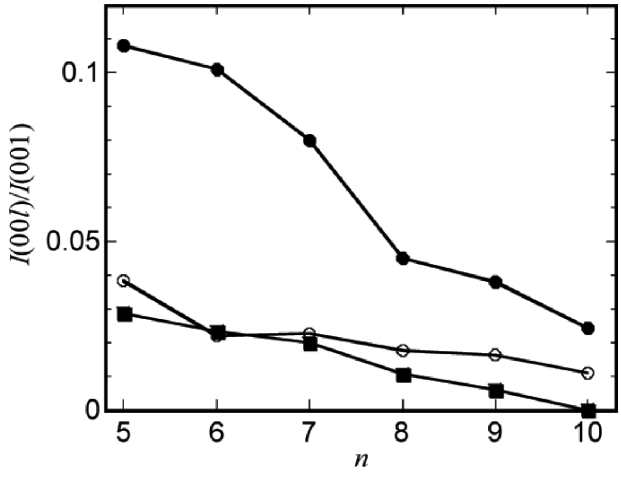

Figure 12. Variation of the intensity ratios of *l*th-order smectic layer reflections with *n*. *I*(002)/*I*(001) (circles) and *I*(003)/*I*(001) (squares) for C-*n* (closed symbols) and L-*n* (open symbols) dimers. *I*(003)/*I*(001) cannot be evaluated for L-*n* because of the weak intensity of the (003) reflection.

On the other hand, a large intensity ratio is observed in the C-*n* dimers, and the ratio depends strongly on *n*. When compared in a homologous series, a higher intensity ratio of *I*(002)/*I*(001) means a higher layer order parameter. Hence, the smectic layer order in C-*n* dimers decreases with increasing of *n*. In other words, the entropy change related to the disappearance of the SmA layer order will decrease with *n*. This decrease may exceed the expected increase in entropy change due to the conformation change in C-*n* dimers, leading to the unusual *n* dependence observed in Figure 8. It is interesting that the smectic phase in C-*n* dimers possesses much higher layer order than that in L-*n* dimers, especially when *n* is small. This difference may be due to the high rigidity of the C-*n* molecules. The C-*n* dimers

may behave as totally rigid molecules rather than partly rigid ones such as the L-*n* dimers.

4. Conclusions

Smectic dimers having allyl tails were synthesised and their tails were connected by ring-closing metathesis under high dilution in the presence of the first Grubbs catalyst to obtain macrocyclised dimers (C-*n*). The C-*n* dimers form a smectic phase similarly to the precursor L-*n* dimers, but significant characteristics of LC behaviour of C-*n* dimers are found, which differ from those of the precursor L-*n* dimers. First, the C-*n* dimers invariably form SmA phases, although the L-*n* dimers as well as the conventional dimers form SmA and SmCA phases depending on whether the carbon numbers on the spacer is even or odd. Second, the isotropisation temperature of the smectic phase is significantly higher than that of the L-*n* dimers and as a result, the smectic temperature span is expanded to 100°C from approximately 30°C of L-*n*. Third, the smectic phase of the C-*n* dimers exhibit a layer order markedly higher than that of L-*n* dimers, particularly when *n* is small. These differences are attributed to the macrocyclisation, which forces the spacer to fold and the two mesogens within a molecule to face each other at a short distance. Hence, the cyclic dimer behaves as a totally rigid molecule in which the conformational diversity is not large for the isotropisation of the smectic phase. Such rigid or restricted conformations are suggested from the significant upfield shift of the aromatic protons in ^{1}H-NMR of the solutions.

Acknowledgements

This research was supported by the Grant-in-Aid for Creative Scientific Research from the Ministry of Education, Science, Sports and Culture, Japan.

References

(1) Imrie, C.T.; Henderson, P.A. *Chem. Soc. Rev.* **2007**, *36*, 2096–2124.
(2) Watanabe, J.; Komura, H.; Niiori, T. *Liq. Cryst.* **1993**, *13*, 455–465.
(3) Watanabe, J.; Hayashi, M.; Nakata, Y.; Niori, T.; Tokita, M. *Prog. Polym. Sci.* **1997**, *22*, 1053–1087.
(4) Izumi, T.; Kang, S.; Niori, T.; Takanishi, Y.; Takezoe, H.; Watanabe, J. *Jpn. J. Appl. Phys.* **2006**, *45*, 1506–1514.
(5) Naito, Y.; Ishige, R.; Itoh, M.; Tokita, M.; Watanabe, J. *Chem. Lett.* **2008**, *37*, 880–881.
(6) Tezuka, Y.; Komiya, R. *Macromolecules* **2002**, *35*, 8667–8669.
(7) Tezuka, Y.; Ohtsuka, T.; Adachi, K.; Komiya, R.; Ohno, N.; Okui, N. *Macromol. Rapid Commun.* **2008**, *29*, 1237–1241.
(8) Grubbs, R.H.; Chang, S. *Tetrahedron* **1998**, *54*, 4413–4450.
(9) Ashton, P.R.; Joachimi, D.; Spencer, N.; Stoddart, J.F.; Tschierske, C.; White, A.J.P.; Williams, D.; Zab, K. *Angew. Chem. Int. Ed. Engl.* **1994**, *33*, 1503–1506.
(10) Joachimi, D.; Ashton, P.R.; Sauer, C.; Spencer, N.; Tschierske, C.; Zab, K. *Liq. Cryst.* **1996**, *20*, 337–348.
(11) Hegmann, T., Neumann, B.; Wolf, R.; Tschierske, C. *J. Mater. Chem.* **2005**, *15*, 1025–1034.
(12) Percec, V.; Turkaly, P.J.; Asandei, A.D. *Macromolecules* **1997**, *30*, 943–952.
(13) Percec, V.; Kawasumi, M.; Rinaldi, P.L.; Litman, V.E. *Macromolecules* **1992**, *25*, 3851–3861.
(14) Watanabe, J.; Hayashi, M. *Macromolecules* **1989**, *22*, 4083–4088.